https://dx.doi.org/10.21577/0103-5053.20200131

J. Braz. Chem. Soc., Vol. 31, No. 11, 2351-2359, 2020
Printed in Brazil - ©2020 Sociedade Brasileira de Química

Article

Nickel-Cerium Layered Double Hydroxide as Electrocatalyst for Glycerol Oxidation

Geovanne L. de Assis,[*,a] *Josué M. Gonçalves,*[a] *Juliana S. Bernardes*[b] *and Koiti Araki*[a]

[a]*Departamento de Química Fundamental, Instituto de Química, Universidade de São Paulo, Av. Prof Lineu Prestes, 748, 05508-000 São Paulo-SP, Brazil*

[b]*Laboratório Nacional de Nanotecnologia (LNNano), Centro Nacional de Pesquisa em Energia e Materiais (CNPEM), Rua Giuseppe Máximo Scolfaro, 10000, 13083-970 Campinas-SP, Brazil*

A new nickel based layered double hydroxide nanomaterial, $Ni_{0.8}Ce_{0.2}$-LDH, constituted by about 3 nm large nanoparticles exhibiting enhanced electrocatalytic properties towards oxidation of glycerol in alkaline media, was prepared by incorporation of 20 wt.% of Ce^{III} ions into α-nickel hydroxide. This can be oxidized to Ce^{IV}, as demonstrated by X-ray photoelectron spectroscopy, a much electron withdrawing and oxidizing species responsible for electronic interactions and additional electrocatalytic active sites giving rise to synergic effects. High-resolution transmission electron microscopy images and the X-ray diffractograms indicated a material with a significantly lower size and degree of crystallinity than α-$Ni(OH)_2$, one of the factors contributing to its enhanced electrochemical and electrocatalytic activity, as demonstrated by cyclic voltammetry and electrochemical impedance spectroscopy, suggesting a good potentiality for development of glycerol fuel cells.

Keywords: glycerol oxidation, nanostructured materials, NiCe-hydroxide, layered double hydroxides, α-$Ni(OH)_2$, electrocatalyst

Introduction

The increasing energy demand and the limited availability of fossil fuels are pushing the development of higher performance and environmentally friendly energy conversion and storage devices, which are one of the key technological challenges in the 21st century.[1] Fuels cells, electrochemical devices that convert chemical energy directly into electric energy, are promising alternatives to rechargeable batteries,[2] especially when cheap byproducts such as glycerol is employed.

One type of fuel cell, a direct glycerol fuel cell (DGFC) using glycerol or glycerol solution as fuel and proton source is attractive because its storage is much simple and safe as compared with hydrogen gas.[3] Moreover, glycerol is widely available from biodiesel production, being a resource produced in a renewable, more environmental-friendly, and cost effective manner.[4] In addition, its electrooxidation in DGFCs cogenerate electricity and large amounts of high value chemicals[5] as byproducts that can be utilized in the pharmaceutical, food, cosmetics and tobacco industries.[6] In fact, many investigations have been conducted on glycerol oxidation exploring different types of electrode materials.[7] Therefore, many research groups are focused on the development of electrocatalytic materials for this type of device. One class of such materials are the layered nanomaterials, that have attracted great attention due to the large interplanar distances that facilitate the intercalation of several compounds into the precursor materials, as well as their large surface areas[8] and surface concentrations of active sites, favoring the diffusion of reactants and enhanced catalytic performance.

Among the layered transition metal oxides and hydroxides, $Ni(OH)_2$ constitutes a class of electrocatalytic and electrochromic materials that have been extensively used in rechargeable batteries,[9] hybrid supercapacitors,[10] sensors[11,12] and fuel cells.[13] In fact, $Ni(OH)_2$ nanoparticles (NPs) wrapped by poly[Ni(salen)] film (Ni(salen): *N*,*N*'-bis(salicylidene)-ethylenediaminonickel(II) complex) was investigated as electrocatalyst for oxidation of methanol, ethanol and glycerol in alkaline electrolyte by Bott-Neto *et al.*[7] The results show that the Ni^{II}-salen complex can be used as precursor of $Ni(OH)_2$ based NP catalysts with average diameter of 2.4 nm, uniformly dispersed in the polymeric matrix. *In situ* Fourier transform infrared (FTIR)

*e-mail: geovannelemos@usp.br
Dedicated to Prof Henrique Eisi Toma on the occasion of his 70th birthday.

spectroscopy studies confirmed that the electrocatalytic oxidation of those alcohols is dependent on the formation of the β-NiOOH species, and the oxidation products are similar to those produced in other nickel-based electrodes. In other words, β-NiOOH species is the electrocatalytic active species responsible for the oxidation of alcohols thus regenerating β-$Ni(OH)_2$. However, it is important to highlight that the materials in the alpha phase (α-$Ni(OH)_2$) exhibit a much more disorganized structure but higher electrocatalytic activity and specific charge capacity.[14] Accordingly, the efficiency of alkaline fuel cells and energy storage devices tend to decrease as it is converted to crystalline β-$Ni(OH)_2$.[15,16]

Several studies have shown that the structural stability and electrochemical performance of modified α-$Ni(OH)_2$ are better than that of neat α-$Ni(OH)_2$.[17] In fact, several studies have been carried out focusing on the isomorphic substitution of Ni^{II} by others M^{II} metal cations such as Co^{II},[18] Mn^{II},[19] and Zn^{II},[9] generating materials denominated double hydroxide salts (DHSs) and described by the general formula $M^a_{1-x}M^b_x(OH)_{2-x}(A^{m-})_{x/m}{\cdot}nH_2O$, where M^a and M^b are divalent metal cations. On the other hand, the incorporation of M^{III} ions such as Al^{III},[20,21] Co^{III},[22] Fe^{III},[23,24] and Ce^{III},[25] results in the formation of layered double hydroxides (LDHs) represented by the general formula $[M1^{II}_{1-x}M2^{III}_x(OH)_2]_x^+(A^{m-})_{x/m}{\cdot}nH_2O$, where $M1 = Ni^{II}$ and $M2^{III}$ are different metal cations in 3+ oxidation state, and A is the counter ion.[26,27]

In addition to increased stability, the DHSs and LDHs materials exhibit enhanced synergistic electrochemical properties. In this sense, Ce^{III} based layered nanomaterials have also attracted much attention due to its high chemical stability, and excellent electric conductivity.[28-30] In fact, Xu *et al.*,[31] developed Ce^{III} doped NiFe-LDH/CNT (CNT: carbon nanotube) nanoarrays by *in situ* self-assembly at room temperature. The ternary NiFeCe-LDH/CNT electrocatalyst obtained in such a way displayed high OER (oxygen evolution reaction) activity and a substantially lower overpotential (227 mV at 10 mA cm^{-2}) and Tafel slope (33 mV dec^{-1}) in alkaline medium, competing favorably with NiFe-based LDHs, and outperforming commercial Ir/C catalysts. The OER activity of the nanocomposite was significantly enhanced mainly because of the much larger specific surface area, high density of lattice defects, much better electron transport efficiency, and synergetic effects associated with the redox properties and larger coordination number of Ce^{III} incorporated in the layered nanostructure.

Accordingly, Ce-based LDHs are known to be excellent electrocatalytic materials because of its ability to store and transfer an oxygen atom concomitantly with an oxidation equivalent as expected for the reversible Ce^{IV}/Ce^{III} process, its high oxygen carrying capacity and low price.[32,33] In this context, hereon we describe the preparation, characterization and enhanced electrocatalytic properties of a new $Ni_{0.8}Ce_{0.2}$-LDH and evidence for a possible direct participation of that rare earth ion in the glycerol electrooxidation reaction, in 1.0 mol L^{-1} NaOH.

Experimental

Materials and methods

Cerium(III) acetate ($Ce(CH_3COO)_3.xH_2O$, purity ≥ 99.9%, Sigma-Aldrich, Saint Louis, USA), nickel(II) acetate tetrahydrate ($Ni(CH_3COO)_2.4H_2O$, purity ≥ 99.0%, Sigma-Aldrich, Saint Louis, USA), *n*-butyl alcohol ($CH_3(CH_2)_3OH$, purity ≥ 99.5%, Merck, Darmstadt, Germany), glycerol ($C_3H_8O_3$, purity ≥ 99.5%, Synth, Diadema, Brazil), potassium hydroxide (KOH, purity ≥ 86.1%, Neon comercial, Suzano, Brazil), sodium hydroxide (NaOH, purity ≥ 97.9%, Synth, Diadema, Brazil) and isopropyl alcohol ($(CH_3)_2CHOH$, purity ≥ 99.5%, Synth, Diadema, Brazil) were used as received, without further purification.

Preparation of α-$Ni(OH)_2$ and α-$Ni_{0.8}Ce_{0.2}$-LDH nanoparticles

Sol suspensions of pure α-$Ni(OH)_2$ and Ce-incorporated α-$Ni(OH)_2$ (α-$Ni_{1-x}Ce_x$-LDH, where x = 0.05, 0.1 and 0.2) NPs were prepared in the stabilized α crystalline phase. The NiCe-LDH materials with increasing concentrations of Ce^{III} ions exhibited similar structures and increasingly larger electrocatalytic activity but that become significantly larger only in $Ni_{0.8}Ce_{0.2}$-LDH as can be seen in the Figure S1 (Supplementary Information (SI) section), reason why now on this work will be focused on it. The α-$Ni(OH)_2$ NPs were prepared by dissolving 4.82 mmol of the nickel acetate in 25.0 mL of glycerol and adding stoichiometric amounts of KOH in *n*-butanol solution (9.64 mmol dissolved in 18.0 mL of *n*-butanol was added dropwise) at room temperature, according to a previously described procedure.[34,35] The $Ni_{0.8}Ce_{0.2}$-LDH samples were prepared in a similar way by reacting a solution of nickel acetate (3.86 mmol) and cerium acetate (0.96 mmol) in 25.0 mL of glycerol with stoichiometric amounts of KOH in *n*-butanol solution (10.60 mmol in 18.0 mL of *n*-butanol). This solution was very quickly added into the former one at room temperature.

Preparation of α-$Ni(OH)_2$ and $Ni_{0.8}Ce_{0.2}$-LDH modified FTO electrodes

FTO (fluorine doped tin oxide) glass pieces (1.0 × 2.5 cm) were carefully washed with soap and rinsed with isopropanol

and water. Then, a 1 cm^2 area was delimited on the surface with a scotch tape and 50 μL of a nanomaterial suspension was spin-coated, the tape removed and the modified electrode heated at 240 °C, for 30 min, to produce adherent and mechanically stable films.

Characterization

The samples were characterized by X-ray diffractometry (XRD) in a Bruker D2 Phaser equipment (Germany) with a Cu Kα source (λ = 1.5418 Å, 30 kV, 15 mA, step = 0.05º) and air-scatter screens to avoid diffuse scattering at lower angles, in the 2θ range from 5 to 70º. Samples were prepared on glass substrates by depositing 50 μL of a nanoparticle suspension and heating at 240 °C for 30 min.

Chemical surface analyses were carried out by X-ray photoelectron spectroscopy (XPS), using a K-α X-ray photoelectron spectrometer (Thermo Fisher Scientific, UK) equipped with a hemispherical electron analyzer and monochromatic Al Kα (1486.6 eV) radiation source. Survey (full-range) and high-resolution spectra of Ce and Ni were acquired using pass energy of 200 and 50 eV, respectively, and the data analyses carried out using the Thermo Avantage Software (version 5.921). The XPS results presented in this work correspond to the average of at least three independent measurements performed in different regions of each sample.

Transmission electron microscopy (TEM) and high-resolution transmission electron microscopy (HRTEM) images were obtained in a JEOL JSM-FEG 7401F equipment (Japan), at an accelerating voltage of 200 kV. Samples were prepared on copper grids (Ted Pella) by dispersing 3 μL of a nanoparticle suspension diluted in deionized water.

Electrochemical measurements

All electrochemical measurements were conducted using a PGSTAT 30 electrochemical workstation (Autolab, Metrohm, Netherlands) and a classical three electrodes configuration cell at room temperature, and a 1.0 mol L^{-1} NaOH aqueous solution as electrolyte. FTO electrodes modified with α-$Ni(OH)_2$ and $Ni_{0.8}Ce_{0.2}$-LDH were employed as the working electrode (Figure S2, SI section), while a platinum foil and Ag/AgCl (KCl, 3.0 mol L^{-1}) were respectively used as the counter and reference electrodes.

The activity of the nanocatalysts for glycerol electrooxidation was measured by cyclic voltammetry in 1.0 mol L^{-1} NaOH solution containing 1.9 mmol L^{-1} of glycerol, at room temperature. The CV curves were recorded in the potential range from 0.10 to 0.55 V, at scan rate of 50 mV s^{-1}.

The electrochemical impedance spectra were recorded at 0.5 V using the same electrochemical arrangement, modulating the frequency of the sinusoidal potential wave (amplitude = 10 mV) superimposed to the AC potential from 100 kHz to 0.01 Hz.

Results and Discussion

Physicochemical characterization

TEM images were used to estimate the α-$Ni(OH)_2$ and $Ni_{0.8}Ce_{0.2}$-LDH nanoparticles size and morphology using samples prepared by depositing them on graphene oxide sheets, as shown in Figure 1. It is interesting to note that $Ni_{0.8}Ce_{0.2}$-LDH NPs are much smaller suggesting that Ce^{III} ions probably are introducing a significant local distortion/stress to the lattice generating defective sites. A similar influence of cerium ions has also been observed by Xu *et al.*[31] in the NiFeCe-LDH/CNT composite, in which 5 wt.% of Ce^{III} ions was shown to be enough to reduce the average NPs size. It is worth noting here the possibility of $Ni_{0.8}Ce_{0.2}$-LDH conversion to $(NiCe)O_x$ by the electron beam due to the local heating and the high vacuum in the sample chamber, generating oxide NPs.[36]

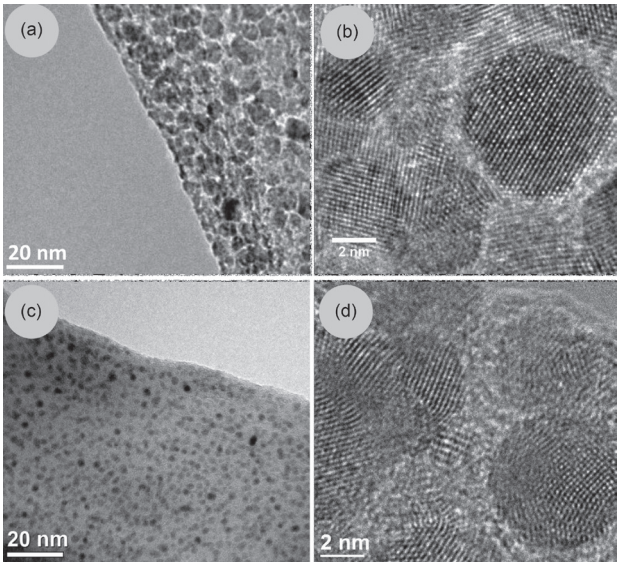

Figure 1. TEM and HRTEM images of (a, b) α-$Ni(OH)_2$ and (c, d) $Ni_{0.8}Ce_{0.2}$-LDH.

In our work, 20 wt.% of Ce^{III} ions in α-$Ni(OH)_2$ decreased the nanoparticle size from 6 to ca. 3 nm. Such effect can be ascribed to the contrasting NPs nucleation rates and/or lattice distortion caused by the Ce^{III} ions. In fact, a faster nucleation can favor the growth of smaller crystals, as previously demonstrated for incorporation of lanthanide ions.[37] In addition, the incorporation of much

larger Ce^{III} (102 pm as compared to 72 pm of Ni^{II}) ions into $Ni(OH)_2$ producing $Ni_{0.8}Ce_{0.2}$-LDH tend to generate local stress and lattice distortions that may hamper the growth of layered double hydroxide nanocrystals.

The structural information of $Ni(OH)_2$ and $Ni_{0.8}Ce_{0.2}$-LDH NPs was obtained by XRD measurements, as shown in the diffractograms of the respective samples prepared by depositing the materials on glass substrates (Figure 2). The $Ni(OH)_2$ sample presented a peak at 10.50° which can be indexed to the (003) plane characteristic of the material in the α-phase.[38] In fact, this is the most characteristic feature of the significantly more disordered α-phase material, as compared to the crystalline β-phase material exhibiting several sharp peaks in the diffractogram. Similarly, considering an isomorphic substitution of Ni^{II} by Ce^{III} ions, the main diffraction peak of $Ni_{0.8}Ce_{0.2}$-LDH at 10.42º was assigned to the respective layered double hydroxide material. The incorporation of Ce^{III} ions (102 pm), much larger than Ni^{II} (72 pm), did not change significantly the interplanar distances, and the basal spacing of α-$Ni(OH)_2$ (d_{003} ca. 0.84 nm) was not significantly increased in $Ni_{0.8}Ce_{0.2}$-LDH (d_{003} ca. 0.86 nm). Nevertheless, the clearly apparent lower intensity and broadness of that XRD peak is characteristic of a less crystalline material, and/or a material constituted by smaller size particles, as expected. The formation of $Ni_{0.8}Ce_{0.2}$-LDH nanoparticles was confirmed by STEM (scanning transmission electron microscopy), where the bright field image (Figure S4a, transmitted electrons, BF) and dark field (Figure S4b, scattered in high-angle annular dark field, HAADF) exhibited similar contrast and no clear indication of segregation of the $Ni(OH)_2$ and $Ce(OH)_3$ phases.[25] These results indicates that 20 wt.% of Ce^{III} ions was incorporated into the α-$Ni(OH)_2$ lattice without any segregation or phase separation, generating a completely homogeneous material, demonstrating the suitability of the sol-gel method. In fact, this method is attracting considerable attention because employs mild conditions and allows good and easy control of the structure, composition and the degree of homogeneity.[38]

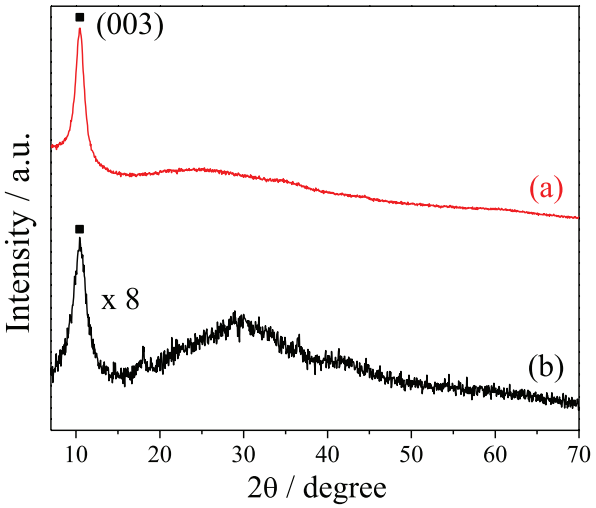

Figure 2. X-ray diffractograms of (a) α-$Ni(OH)_2$ and (b) $Ni_{0.8}Ce_{0.2}$-LDH nanoparticles deposited on a glass substrate.

The eventual presence of nickel hydroxide derivative in the more organized β phase was further evaluated by FTIR data as shown in SI section (Figure S5). The broad band at 650 cm^{-1} in the α-$Ni(OH)_2$ spectrum is characteristic of the δ(OH), but this same IR-active band appears at 500 cm^{-1} in β-$Ni(OH)_2$,[39,40] confirming the presence of nickel hydroxide in the α-phase. The incorporation of Ce^{III} ions into α-$Ni(OH)_2$ decreased the intensity of that band and led to appearance of two sharper bands at 605 and 669 cm^{-1} probably associated with δ(OH) bond to cerium and nickel sites next to cerium ions as expected for the NiCe-LDH material. In addition, the two bands at 1558 and 1417 cm^{-1} has been assigned to ν_a(OCO) and ν_s(OCO) stretching vibrations of organic acid anions, respectively,[41] and that at 1383 cm^{-1} must be assigned to δ(CH) or ρ_r(COO) stretching/bending vibrations of CH and carboxylate groups,[7] respectively. These carboxylate-containing species were probably produced during the heat treatment of the samples (α-$Ni(OH)_2$ and NiCe-LDH films) by oxidative breakdown of glycerol molecules, which were used as solvent during the synthetic procedure, thus generating smaller compounds such as carbonate and oxalate. As reported by Rives,[42] the presence of intercalated carbonate and oxalate anions in these class of compounds induce interlayer spacing about 0.80 nm for carbonate and in the range of 0.80-0.90 nm for oxalate anions, which are in accordance with the present work (0.84 and 0.86 nm). However, the presence of interlayered acetate anions (from precursor salts) coordinated perpendicularly to the plane of the layer has been ruled out, since which would increase the interlamellar spacing to ca. 1.30 nm as described by Choy *et al.*[43]

XPS measurements were carried out for determination of the valence states of Ni and Ce in the nanomaterial. The Ni 2p region of α-$Ni(OH)_2$ and $Ni_{0.8}Ce_{0.2}$-LDH (Figure 3a) shows the typical Ni^{II} peaks respectively at 873.7 eV (Ni $2p_{1/2}$) and 855.9 eV (Ni $2p_{3/2}$), and 873.3 eV (Ni $2p_{1/2}$) and 855.7 eV (Ni $2p_{3/2}$), with their corresponding satellites, in good agreement with the spectrum of a standard α-$Ni(OH)_2$ sample exhibiting peaks at 873.3 eV (Ni $2p_{1/2}$) and 855.6 eV (Ni $2p_{3/2}$). The Ce 3d high resolution spectrum (Figure 3b) exhibits the Ce $3d_{3/2}$ and Ce $3d_{5/2}$ peaks respectively at 904.0 and 885.3 eV,[31] confirming the presence of Ce^{III} in $Ni_{0.8}Ce_{0.2}$-LDH. However, there is a positive shift of 1.3 eV as compared to that of $Ce(OH)_3$

reference, indicating a significantly lower electron binding energy for the Ce^{III} ions as expected for the presence of less electronegative Ni^{II} ions bond next to them. Also, it is interesting to note that a weak peak characteristic of CeO_2 like sites appeared at 917 eV after heat treatment at 240 ºC for 30 min (Figure 3c) indicating that site is available for redox processes. This is a very interesting feature since Ce^{IV} is an potent oxidizing species that besides creating new catalytic active sites may induce synergic effects enhancing the electrocatalytic activity of the NiCe-LDH material for oxidation reactions, as compared to pure α-$Ni(OH)_2$.

Electrochemical properties

The electrochemical performance of α-$Ni(OH)_2$ and $Ni_{0.8}Ce_{0.2}$-LDH NPs modified FTO electrodes were evaluated by cyclic voltammetry (CV) measurements within a potential window from 0.10 to 0.55 V (*vs*. Ag/AgCl 3.0 mol L^{-1}) in aqueous 1.0 mol L^{-1} NaOH solution. The electrochemical behavior during 100 CV cycles at 50 mV s^{-1} is shown in Figure 4. Note that both materials present an increase in the current as a function of the number of CV cycles. This behavior was attributed to the progressive diffusion of the electrolyte solution into the nanomaterial activating more and more Ni^{II} sites, as previously reported.[44] The oxidation peak was found at 0.43 V (*vs*. Hg/HgO, KOH 1 M), a potentially typically assigned to the α-nickel hydroxide materials, while that peak appears shifted to potentials more positive than about 0.5 V (*vs*. Hg/HgO, KOH 1 M) in the β phase material.[45]

It is easy to see that the $Ni_{0.8}Ce_{0.2}$-LDH/FTO electrode exhibits much broad waves than the α-$Ni(OH)_2$/FTO electrode but with similar peak currents, indicating that the amount of exchanged electrons is much larger, or in other words, that the concentration of redox active sites is much larger. This is a very important feature of an electrocatalyst and the wave broadening suggests that the activated Ni^{II} sites probably are in different chemical environments in the LDH lattice. Such a broadening can also be consequence of the resistance to electrolyte diffusion as observed when the thickness of the film deposited on FTO was increased, as previously reported,[25] but this is not the case here. The anodic peak at around 0.35 V is attributed to the oxidation of α-$Ni(OH)_2$ to γ-NiOOH, while the cathodic peak at 0.26 V is related to the reverse reaction, according to the following electrochemical process:[46,47]

$$\alpha\text{-}Ni(OH)_2 + OH^- \rightarrow \gamma\text{-}NiOOH + H_2O + e^- \quad (1)$$

The electrocatalytic activity of α-$Ni(OH)_2$ and $Ni_{0.8}Ce_{0.2}$-LDH modified FTO electrodes for oxidation of glycerol was investigated by cyclic voltammetry in 1.0 mol L^{-1} NaOH solution (Figures 5a and 5c) since LDH derivatives prepared with lower Ce^{III} content did not exhibit significantly larger electrocatalytic activity as compared to pure α-nickel hydroxide (Figure S1, SI section). The CV curves in the presence of 1.9 mmol L^{-1} of glycerol clearly demonstrates the much larger electrocatalytic activity of the LDH material, which presented 1.7 times larger current at 0.50 V.

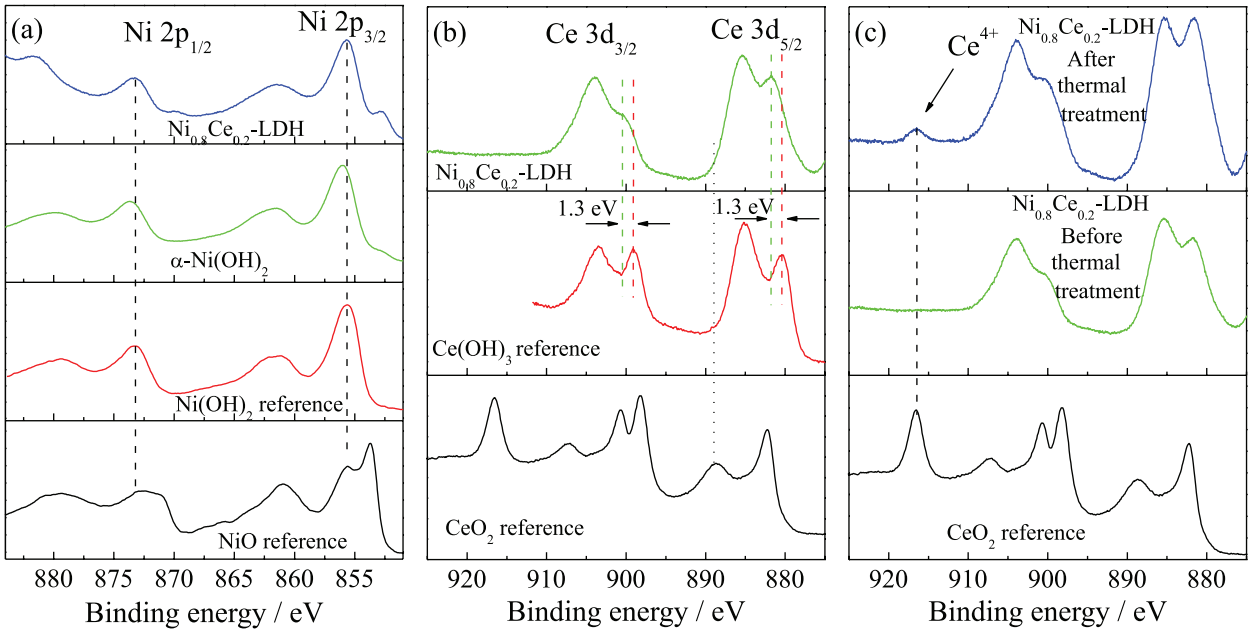

Figure 3. High resolution XPS spectra of α-$Ni(OH)_2$ and $Ni_{0.8}Ce_{0.2}$-LDH in the (a) Ni 2p region, and (b) Ce 3d region, and (c) of $Ni_{0.8}Ce_{0.2}$-LDH before and after calcination at 240 ºC for 30 min.

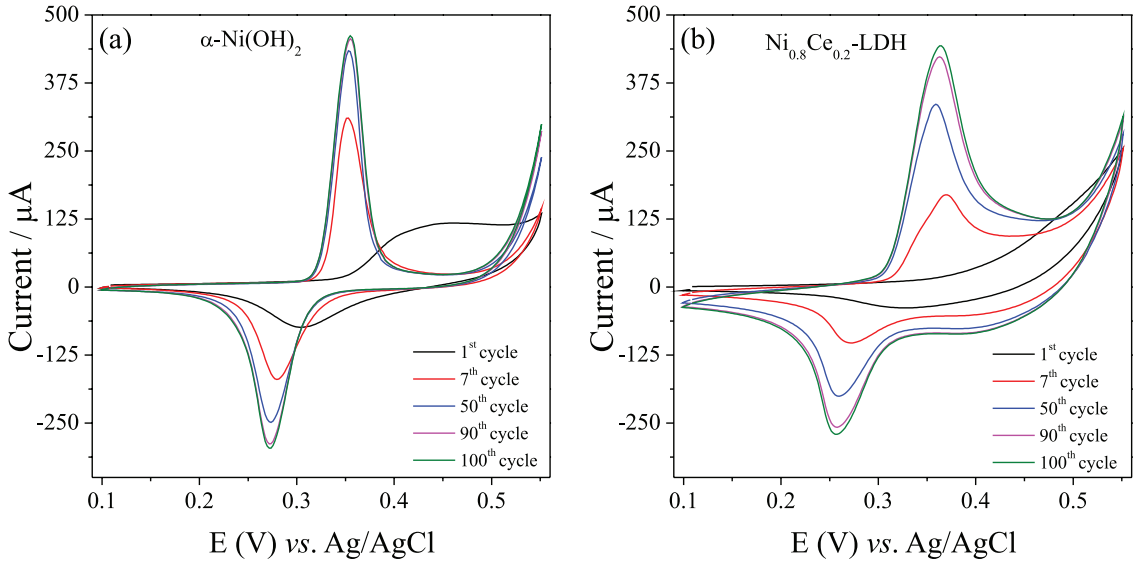

Figure 4. Cyclic voltammograms of (a) α-$Ni(OH)_2$ and (b) $Ni_{0.8}Ce_{0.2}$-LDH modified FTO electrodes as a function of the number of cycles in 1.0 mol L^{-1} NaOH solution, at 50 mV s^{-1}.

Accordingly, electrochemical impedance spectroscopy (EIS) measurements were performed to clarify the electrochemical properties at 0.50 V, using an amplitude AC perturbation of 10 mV, in the 0.01 Hz to 100 kHz range, and the respective Nyquist plots are shown in Figures 5b and 5d. The equivalent circuit used to fit the experimental data is shown in the inset of Figure 5d, in which R_s represents the combined resistance of the electrolyte, the intrinsic resistance of FTO, and the contact resistance of the nanomaterials with the FTO substrate; R_1 represents the charge-diffusion resistance in the modified electrodes, and R_2 the heterogeneous charge-transfer resistance for oxidation of glycerol (or water) on the electrode surface. The impedance parameters obtained by fitting the experimental data are listed in Table 1.

The R_1 values are relatively low as expected spanning the 7.1 to 12.0 ohms range, whilst R_2 was significantly different for α-$Ni(OH)_2$ and $Ni_{0.8}Ce_{0.2}$-LDH, in the absence and presence of glycerol. In fact, the heterogeneous charge-transfer resistance decreased from about 367 ohms in the pure nickel hydroxide to 230 ohms in the LDH material, as expected for its higher electrocatalytic activity. In addition, it is relevant to mention the quite significant decrease of such parameter, from 230 to 185 ohms for LDH (and from 367 to 344 ohms for α-$Ni(OH)_2$) upon addition of glycerol, indicating that this compound is more easily oxidized than water.[48,49] Such an improvement in performance suggests that the presence of Ce^{III} ions in the LDH material is beneficial and is increasing the heterogeneous charge-transfer kinetics. The possibility of improvement of the materials conductivity can be ruled out since no significant change of R_1 was observed upon incorporation of 20 wt.% of Ce^{III} in the α-$Ni(OH)_2$ matrix (Table 1).

As pointed out previously, Ce^{III} ion is much larger than the Ni^{II} ion and can induce local structural distortions that can enhance the activity of the nickel sites. However, we demonstrated by XPS that the Ce^{III} ions can also be oxidized to Ce^{IV} ions in the NiOOH structure, a species that is well-known for its oxidizing properties. Accordingly, the glycerol electrooxidation mechanism may include the simultaneous action of both, the nickel and cerium sites. First, both sites are activated by oxidation to their respective higher valence states, then the electrochemically generated Ni^{III} and Ce^{IV} species oxidize glycerol and are reduced back regenerating the starting species, according to equations 2-5. Thus, the enhanced electrocatalytic activity was attributed to lattice distortions and the presence of catalytic active Ce^{IV} sites, that can act in parallel or synergistic way. This last hypothesis is considered more probable given its very high electron withdrawing and electronegativity that also can activate further the electrocatalytic activity of the nickel sites for oxidation reactions.

$$Ni(OH)_2 + OH^- \rightarrow NiOOH + H_2O + e^- \quad (2)$$

$$NiOOH + Glycerol \rightarrow products + Ni(OH)_2 \quad (3)$$

$$Ce(OH)_3 + OH^- \rightarrow CeO_2 + 2H_2O + e^- \quad (4)$$

$$CeO_2 + Glycerol \rightarrow products + Ce(OH)_3 \quad (5)$$

To better evaluate the electrocatalytic activity of α-$Ni(OH)_2$ and NiCe-LDH electrodes toward glycerol oxidation, the results obtained in this work were compared with related works in the literature.[6,7,50,51] As shown in Table 2, the lowest oxidation potential of 0.50 V, that

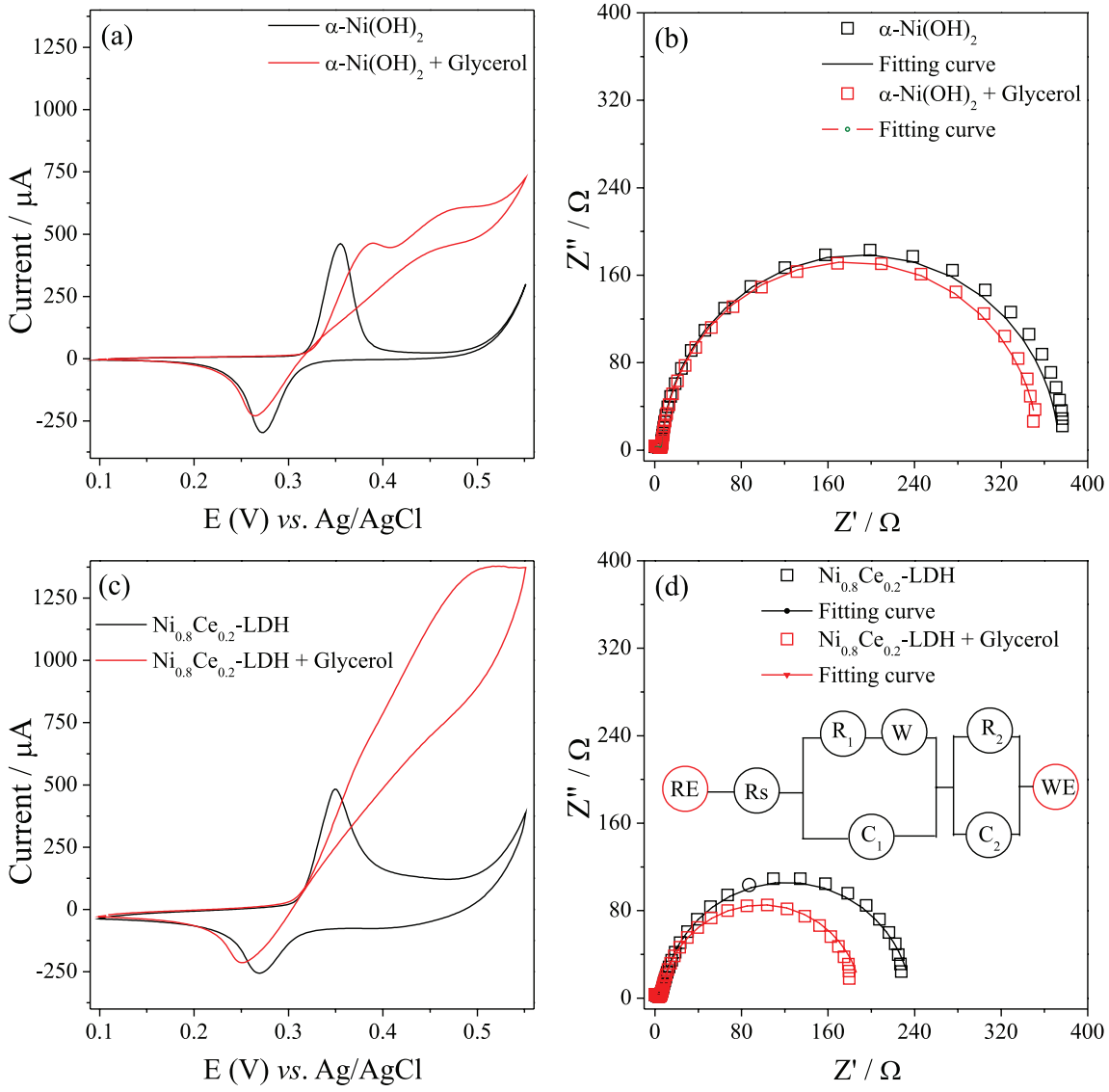

Figure 5. Cyclic voltammograms of (a) α-Ni(OH)$_2$ and (c) $Ni_{0.8}Ce_{0.2}$-LDH modified FTO electrodes in the absence and presence of 1.9 mmol L^{-1} of glycerol in 1.0 mol L^{-1} NaOH electrolyte solution, at 50 mV s^{-1}. Electrochemical impedance spectra recorded at 0.50 V, in the frequency range from 0.01 Hz to 100 kHz to of (b) α-Ni(OH)$_2$ and (d) $Ni_{0.8}Ce_{0.2}$-LDH, and the equivalent circuit used for fitting (inset).

Table 1. EIS data of α-Ni(OH)$_2$ and $Ni_{0.8}Ce_{0.2}$-LDH in the absence and presence of glycerol 1.9 mmol L^{-1}, at AC potential of 0.50 V. Data obtained by fitting of Figures 5b and 5d data

Material	R_s / Ω	R_1 / Ω	R_2 / Ω
α-Ni(OH)$_2$	12.3	7.1	367.0
α-Ni(OH)$_2$ + glycerol	34.0	10.3	344.0
$Ni_{0.8}Ce_{0.2}$-LDH	10.5	10.0	230.0
$Ni_{0.8}Ce_{0.2}$-LDH + glycerol	17.0	12.0	185.0

R_s: combined resistance of the electrolyte, the intrinsic resistance of FTO, and the contact resistance of the nanomaterials with the FTO substrate; R_1: charge-diffusion resistance in the modified electrodes, R_2: heterogeneous charge-transfer resistance for oxidation of glycerol (or water) on the electrode surface; LDH: layered double hydroxides.

indicates a larger electrocatalytic activity, was achieved with the nanomaterials described in this work. The other important parameter is the current density, but this parameter is highly dependent on the substrate concentration and the actual electrode surface area available for the electrocatalytic process and are not directly comparable. In our case, a thin film with relatively low surface area and a 1.9 mM glycerol solution has been considered, while electrodes modified with thicker films with much larger active surface areas and 100 mM glycerol solution was used in the other works. For example, a [Ni(salen)] derivative was electropolymerized on glassy carbon electrode surface generating a thick poly[Ni(salen)]$_{ATV}$ film exhibiting the highest current density of 31.4 mA cm^{-2}. Accordingly, just considering that the substrate concentration is 50 times

Table 2. Electrocatalytic activity of α-$Ni(OH)_2$/FTO and NiCe-LDH/FTO electrodes as compared to related modified electrodes for glycerol electrooxidation reaction

Catalyst	Glycerol solution / mM	E_{pa} / V	j / (mA cm^{-2})	Reference
α-$Ni(OH)_2$	1.9 (1.0 M NaOH)	0.50 (*vs*. Ag/AgCl)	1.1	this work
NiCe-LDH	1.9 (1.0 M NaOH)	0.50 (*vs*. Ag/AgCl)	2.6	this work
Untreated Ni	100.0 (1.0 M KOH)	0.60 (*vs*. Hg/HgO)	4.5	[6]
After treatment Ni	100.0 (1.0 M KOH)	0.60 (*vs*. Hg/HgO)	15.5	[6]
Poly[Ni(salen)]$_{ATV}$	100.0 (1.0 M NaOH)	0.59 (*vs*. Ag/AgCl)	31.4	[7]
Ni-CA	100.0 (1.0 M KOH)	0.55 (*vs*. Ag/AgCl)	10.0	[50]
Ni-TBr	100.0 (1.0 M KOH)	0.55 (*vs*. Ag/AgCl)	8.5	[50]
Ni	100.0 (1.0 M KOH)	0.55 (*vs*. Ag/AgCl)	4.5	[50]
*Ni	100.0 (0.5 M NaOH)	0.70 (*vs*. Ag/AgCl)	20.0	[51]

E_{pa}: anodic peak potential; j: current density; LDH: layered double hydroxides; untreated Ni: untreated nickel wire; after treatment Ni: nickel wire treated in a solution of Na_2SO_4/ascorbic acid; poly[Ni(salen)]$_{ATV}$: *N*,*N*'-bis(salicylidene)-ethylenediaminonickel(II) complex on glassy carbon disk; Ni-CA: nickel electrode-citric acid; Ni-TBr: nickel electrode-tetrabutylammonium bromide; Ni: nickel electrode; *Ni: polycrystalline nickel rod.

larger, the expected current density for NiCe-LDH modified electrodes in the same experimental conditions should be larger than 100 mA cm^{-2}, demonstrating its superior electrocatalytic activity.

Conclusions

The incorporation of Ce^{III} ions into α-$Ni(OH)_2$ lattice influenced the nanoparticles size, degree of crystallinity and electrocatalytic activity of $Ni_{0.8}Ce_{0.2}$-LDH, as demonstrated by TEM, XRD and electrochemical (CV and EIS) measurements. The larger Ce^{III} ions probably are distorting the nickel hydroxide lattice and was shown to be easily oxidized generating Ce^{IV} ion, a highly oxidizing and electron-withdrawing species that can act as additional electrocatalytic active site and induce synergic effects enhancing the electrocatalytic activity of the LDH material for oxidation of organic substrates. In fact, the layered double hydroxide material showed an enhanced electrocatalytic activity 1.7 times larger than α-$Ni(OH)_2$ for oxidation of glycerol, being promising for application in glycerol-based fuel cells.

Supplementary Information

Supplementary data (cyclic voltammetry, electrochemical impedance, ICP-OES (inductively coupled plasma optical emission spectrometry) and FTIR) are available free of charge at http://jbcs.sbq.org.br as PDF file.

Acknowledgments

The authors are grateful to the Brazilian agency Conselho Nacional de Desenvolvimento Científico e Tecnológico-CNPq (processes 131857/2016-9 and 141853/2015-8) for financial support. We also thank Brazilian Nanotechnology National Laboratory-LNNano, CNPEM (Brazil) for the use of TEM and XPS facilities.

References

1. Pawar, S. M.; Inamdar, A. I.; Gurav, K. V.; Jo, Y.; Kim, H.; Kim, J. H.; Im, H.; *Mater. Lett.* **2015**, *141*, 336.
2. Spinacé, E. V.; Neto, A. O.; Vasconcelos, T. R. R.; Linardi, M.; *J. Power Sources* **2004**, *137*, 17.
3. Oliveira, V. L.; Morais, C.; Servat, K.; Napporn, T. W.; Tremiliosi-Filho, G.; Kokoh, K. B.; *J. Electroanal. Chem.* **2013**, *703*, 56.
4. Habibi, B.; Delnavaz, N.; *RSC Adv.* **2016**, *6*, 31797.
5. Coutanceau, C.; Baranton, S.; Kouamé, R. S. B.; *Front. Chem.* **2019**, *7*, 100.
6. Houache, M. S. E.; Cossar, E.; Ntais, S.; Baranova, E. A.; *J. Power Sources* **2018**, *375*, 310.
7. Bott-Neto, J. L.; Martins, T. S.; Machado, S. A. S.; Ticianelli, E. A.; *ACS Appl. Mater. Interfaces* **2019**, *11*, 30810.
8. Zha, D.; Sun, H.; Fu, Y.; Ouyang, X.; Wang, X.; *Electrochim. Acta* **2017**, *236*, 18.
9. Turney, D. E.; Shmukler, M.; Galloway, K.; Klein, M.; Ito, Y.; Sholklapper, T.; Gallaway, J. W.; Nyce, M.; Banerjee, S.; *J. Power Sources* **2014**, *264*, 49.
10. Guo, X. L.; Liu, X. Y.; Hao, X. D.; Zhu, S. J.; Dong, F.; Wen, Z. Q.; Zhang, Y. X.; *Electrochim. Acta* **2016**, *194*, 179.
11. Rinaldi, A. L.; Carballo, R.; *Sens. Actuators, B* **2016**, *228*, 43.
12. Chelaghmia, M. L.; Nacef, M.; Affoune, A. M.; Pontié, M.; Derabla, T.; *Electroanalysis* **2018**, *30*, 1117.
13. Zhu, X.; Dou, X.; Dai, J.; An, X.; Guo, Y.; Zhang, L.; Tao, S.; Zhao, J.; Chu, W.; Zeng, X. C.; Wu, C.; Xie, Y.; *Angew. Chem.* **2016**, *55*, 12465.

14. Yang, X.; Fu, K.; Mao, L.; Peng, W.; Jin, J.; Yang, S.; Li, G.; *Chem. Eng.* **2019**, *205*, 269.
15. Nunes, C. V.; Danczuk, M.; Bortoti, A. A.; Guimarães, R. R.; Gonçalves, J. M.; Araki, K.; Banczek, E. P.; Anaissi, F. J.; *J. Electrochem. Soc.* **2016**, *163*, A2356.
16. Nunes, C. V.; Danczuk, M.; Bortoti, A. A.; Gonçalves, J. M.; Araki, K.; Anaissi, F. J.; *J. Power Sources* **2015**, *297*, 408.
17. Miao, C.; Zhu, Y.; Huang, L.; Zhao, T.; *J. Power Sources* **2015**, *274*, 186.
18. Martins, P. R.; Toma, S. H.; Nakamura, M.; Toma, H. E.; Araki, K.; *RSC Adv.* **2013**, *3*, 20261.
19. Sim, H.; Jo, C.; Yu, T.; Lim, E.; Yoon, S.; Lee, J. H.; Yoo, J.; Lee, J.; Lim, B.; *Chem. Eur.* **2014**, *20*, 14880.
20. Wu, X.-H.; Feng, Q.-P.; Wang, M.; Huang, G.-W.; *J. Power Sources* **2016**, *329*, 170.
21. Ehlsissen, K. T.; Delahaye-Vidal, A.; Genin, P.; Figlarz, M.; Willmann, P.; *J. Mater. Chem.* **1993**, *3*, 883.
22. Chen, H.; Hu, L.; Chen, M.; Yan, Y.; Wu, L.; *Adv. Funct. Mater.* **2014**, *24*, 934.
23. Li, M.; Jijie, R.; Barras, A.; Roussel, P.; Szunerits, S.; Boukherroub, R.; *Electrochim. Acta* **2019**, *302*, 1.
24. Li, Z.; Shao, M.; An, H.; Wang, Z.; Xu, S.; Wei, M.; Evans, D. G.; Duan, X.; *Chem. Sci.* **2015**, *6*, 6624.
25. Gonçalves, J. M.; Guimarães, R. R.; Brandão, B. B. N. S.; Saravia, L. P. H.; Rossini, P. O.; Nunes, C. V.; Bernardes, J. S.; Berttoti, M.; Angnes, L.; Araki, K.; *Electrochim. Acta* **2017**, *247*, 30.
26. Xie, W.; Song, Y.; Li, S.; Shao, M.; Wei, M.; *Energy Environ. Mater.* **2019**, *2*, 158.
27. Indira, L.; Dixit, M.; Kamath, P. V.; *J. Power Sources* **1994**, *52*, 93.
28. Wang, D.; Pang, L.; Mou, H.; Zhou, Y.; Song, C.; *RSC Adv.* **2015**, *5*, 24101.
29. Feng, K.-J.; Yang, Y.-H.; Wang, Z.-J.; Jiang, J.-H.; Shen, G.-L.; Yu, R.-Q.; *Talanta* **2006**, *70*, 561.
30. Ispas, C.; Njagi, J.; Cates, M.; Andreescu, S.; *J. Electrochem. Soc.* **2008**, *155*, F169.
31. Xu, H.; Wang, B.; Shan, C.; Xi, P.; Liu, W.; Tang, Y.; *ACS Appl. Mat. Interfaces* **2018**, *10*, 6336.
32. Zhang, X.; Li, G.; Song, X.; Yang, S.; Sun, Z.; *RSC Adv.* **2017**, *7*, 32442.
33. Suárez-Quezada, M.; Romero-Ortiz, G.; Suárez, V.; Morales-Mendoza, G.; Lartundo-Rojas, L.; Navarro-Cerón, E.; Tzompantzi, F.; Robles, S.; Gómez, R.; Mantilla, A.; *Catal. Today* **2016**, *271*, 213.
34. Rocha, M. A.; Anaissi, F. J.; Toma, H. E.; Araki, K.; Winnischofer, H.; *Mater. Res. Bull.* **2009**, *44*, 970.
35. Martins, P. R.; Rocha, M. A.; Angnes, L.; Toma, H. E.; Araki, K.; *Electroanalysis* **2011**, *23*, 2541.
36. Azeredo, N. F. B.; Rossini, P. O.; Gonçalves, J. M.; Assis, G. L.; Araki, K.; Angnes, L.; *J. Taiwan Inst. Chem. Eng.* **2019**, *95*, 475.
37. Xiang, Y.; Yu, X.-F.; He, D.-F.; Sun, Z.; Cao, Z.; Wang, Q.-Q.; *Adv. Funct. Mater.* **2011**, *21*, 4388.
38. Rocha, M. A.; Winnischofer, H.; Araki, K.; Anaissi, F. J.; Toma, H. E.; *J. Nanosci. Nanotechnol.* **2011**, *11*, 3985.
39. Hall, D. S.; Lockwood, D. J.; Bock, C.; MacDougall, B. R.; *Proc. R. Soc. A* **2015**, *471*.
40. Le Bihan, S.; Figlarz, M.; *J. Cryst. Growth* **1972**, *13-14*, 458.
41. Kowal, A.; Port, S. N.; Nichols, R. J.; *Catal. Today* **1997**, *38*, 483.
42. Rives, V.; *Layered Double Hydroxides: Present and Future*; Nova Science Publishers: New York, USA, 2001.
43. Choy, J.-H.; Kwon, Y.-M.; Han, K.-S.; Song, S.-W.; Chang, S. H.; *Mater. Lett.* **1998**, *34*, 356.
44. Canevari, T. C.; Cincotto, F. H.; Landers, R.; Machado, S. A. S.; *Electrochim. Acta* **2014**, *147*, 688.
45. Kim, M. S.; Kim, K. B.; *J. Electrochem. Soc.* **1998**, *145*, 507.
46. Danczuk, M.; Nunes, C. V.; Araki, K.; Anaissi, F. J.; *J. Solid State Electrochem.* **2014**, *18*, 2279.
47. Módolo, M. L.; Danczuk, M.; Anaissi, F. J.; Araki, K.; Fujiwara, S. T.; *ECS Trans.* **2014**, *61*, 319.
48. Shangguan, E.; Li, J.; Guo, D.; Guo, L.; Nie, M.; Chang, Z.; Yuan, X.-Z.; Wang, H.; *J. Power Sources* **2015**, *282*, 158.
49. Wang, X.; Lin, Y.; Su, Y.; Zhang, B.; Li, C.; Wang, H.; Wang, L.; *Electrochim. Acta* **2017**, *225*, 263.
50. Sivasakthi, P.; Sangaranarayanan, M. V.; *New J. Chem.* **2019**, *43*, 8352.
51. Simpson, D. E.; Juda, K. E.; Roy, D.; *Electrocatalysis* **2018**, *9*, 86.

Submitted: December 8, 2019
Published oinline: June 30, 2020